

3D Cloud Field Retrieval and Data Fusion

L Jones and D Cornford

Department of Computer Science, Aston University,
Birmingham B4 7ET, UK.

Telephone: +44 (0) 121 359 3611 x4667

e-mail: jones11@aston.ac.uk

Abstract

In this paper we present a method for three dimensional cloud field modelling over large, spatially discrete cloud fields using visible spectrum images from geostationary satellite platforms and ground-based cameras. This paper represents work from the first stage of an ongoing project and as such this method uses purely generative image data while applying techniques expected to perform well on real world data at a later date. We use active contours for feature extraction from pre-processed images for both satellite and ground-based data. Relying heavily on computer graphics principles we project features found in ground-based images onto the satellite view for feature matching and cloud base height determination.

1 Introduction

Inference of cloud base height (CBH) is an important part of developing a fully four-dimensional space-time model of the evolving cloud field. Such a model would have application in the verification of numerical weather prediction (NWP) and global climate models (GCM) as well as being a useful tool for nowcasting and operational forecasts. However CBH is a difficult property to establish accurately, particularly for multiple layered clouds and over large spatially discrete cloud fields. Current operational methods of retrieval for CBH are either highly inaccurate such as estimation by cloud type, or are interpolated from point data sources such as radiosondes or the few, unequally distributed ceilometers within the British Isle. Ceilometer data, while accurate, does not penetrate thick clouds and for spatially discrete clouds fields there can be no guarantee that clouds will pass directly over the ceilometer or that temporal properties of the cloud field will be observed. Cloud thickness is also estimated from satellite data, which is capable of retrieving cloud optical thickness, though this suffers from problems created by multiple cloud layers and varying atmospheric and surface properties.

The project, of which this work forms a part, aims to produce a method which utilises current technology in the form of satellite platforms together with cheap ‘off-the-shelf’ digital cameras to produce an easily deployable system with high spatial and temporal resolution. This first stage uses only two images taken from generative data (one satellite and one ground-based view) to develop the methods necessary for migration to Meteosat-7, and eventually Meteosat Second Generation (MSG), visible spectrum data and multi-location ground-based imagery with real world data.

2 Feature Extraction

Feature extraction is a necessary first step in the production of the 3D model. Cloud spatial properties must be found in both satellite and ground-based images before determination of cloud location in 3D space can occur. Cloud profiles in both ground and satellite images are found using active contours [Cohen 1991]. These mutable splines shrink(snakes) or grow(balloons) to fit the profile of a feature in an image. Some pre-processing of the images is required before active contours can be applied. For the generative data it is convenient to use the ‘Canny’ edge detector; as our generative ‘clouds’ have clear, well defined edges this works well, however edge detection on real clouds will produce poor results and it is likely that a gradient vector flow [Xu and Prince 1997] pre-processing method will be used requiring minor adjustment to the active contours algorithms.

2.1 Forces Acting On Active Contours

Active contours use a system of ‘internal’ and ‘external’ forces to mutate a spline through successive iterations. Internal forces act on the spline with no consideration of the image to enforce uniform continuity (smoothness) and control the shrinking or growing of the spline. External forces draw the spline towards features in the image, in our data: pixels of high intensity.

In this work closed non-uniform rational b-splines are used with 30 control points. The internal energy is defined as the weighted sum of two forces, a continuity force and a ballooning force [Mackiewicz 1995].

$$e_{int_i} = k_{cont}e_{cont_i} + k_{ball}e_{ball_i} \quad (1)$$

Where e_{int_i} is the internal energy at control point i , k_{cont} and k_{ball} are the constant weighting factors for continuity and ballooning respectively, and e_{cont_i} and e_{ball_i} are the continuity and ballooning energies at control point i .

$$e_{cont_i} = S \left(l_i \left(\frac{\mathbf{m}_i - G_c}{\|\mathbf{m}_i - G_c\|} \right) + (G_c - G_i) \right) \quad (2)$$

Where G_i is a control point on the spline, G_c is the center of the closed spline, defined by:

$$G_c = \frac{1}{n} \sum_{i=1}^n G_i \quad (3)$$

\mathbf{m}_i is the midpoint between the two control points closest to G_i :

$$\mathbf{m}_i = \frac{G_{i-1} + G_{i+1}}{2} \quad (4)$$

l_i is the mean length of G_{i-1} and G_{i+1} from G_c , and S is the normalisation factor:

$$S = \frac{1}{n} \sum_{i=1}^n \|G_j - G_c\|^2 \quad (5)$$

The ballooning energy force is defined by:

$$e_{ball_i} = (G_i - G_c) \frac{1}{S} \quad (6)$$

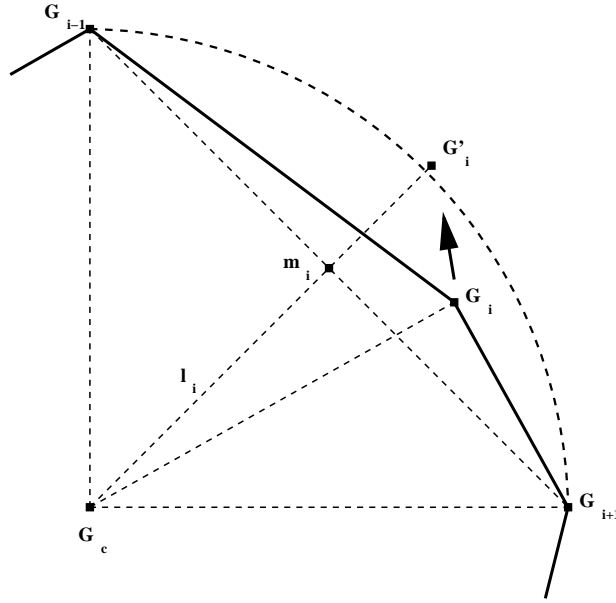


Figure 1: Example of the movement of a point under continuity energy. In the absence of other influences, continuity energy will converge a closed spline to a perfect circle.

External energy is defined by pixel intensities along the vector between the centre of the spline and the control point with a line length of $2r$, where:

$$r = ||G_i - G_c|| \quad (7)$$

The line is parameterised in terms of t , pixel intensities are interpolated at intervals of t using linear scanning interpolation [Blake and Isard 2000] as shown below.

$$I_t = \sum_{i,j} w_{i,j} I_{i,j} \quad (8)$$

$$w_{i,j} = \begin{cases} (1 - |x - i|)(1 - |y - j|), & \text{if } |x - i| < 1 \text{ and } |y - j| < 1 \\ 0, & \text{otherwise} \end{cases} \quad (9)$$

Intensities are weighted according to their ‘closeness’ to the point. The x,y point corresponding to the highest weighted I_t value is taken to be the target for the control point. The external energy for the control point is the movement vector from control point to target point.

3 Vector Creation and Projection

It can be assumed that for any point in a two dimensional image, the corresponding three dimensional point, of which the 2D point is a projection, lies on a line between the centre of the projection and the intersection point of the projection of the 3D point and the view plane.

In computer graphics the view plane is defined by a view-plane reference point (vrp) coordinate, a view up vector (vup) and a view plane normal vector (vpn) defined in 3D space. The centre of the projection is defined in terms of the view plane coordinate system which originates at the vrp and has z axis in the direction of the vpn and y in the direction of the vup projected onto the viewing plane [Foley *et al.* 1997].

For imaging hardware the prp is always on the vpn vector from the vrp . The prp must be transformed

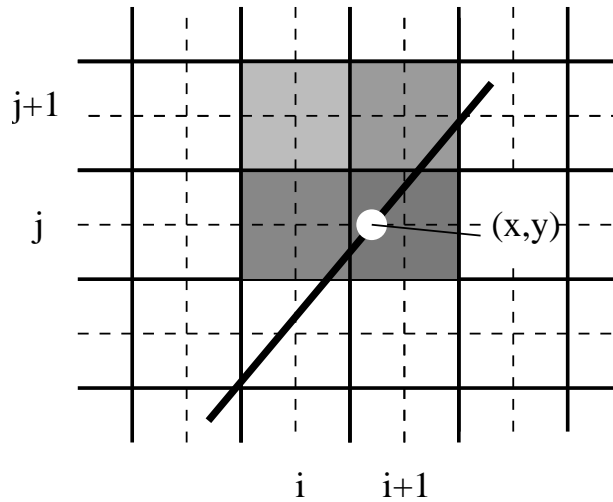


Figure 2: Interpolated Image sampling. The intensity at point (x,y) is a weight sum of I for the four closest pixels, from [Blake and Isard 2000]

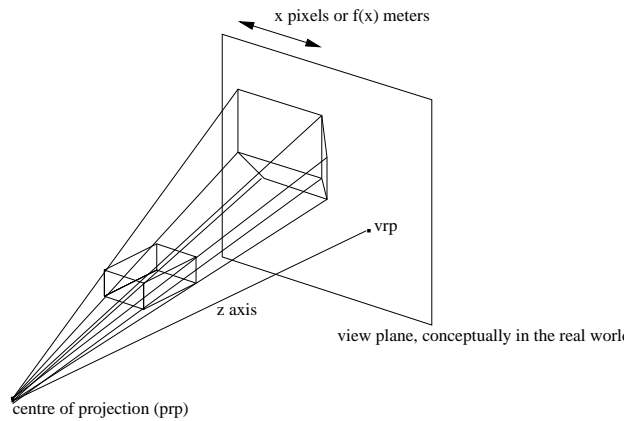


Figure 3: Conceptually the view plane exists in the real world and coordinates can be derived from it.

into world coordinates as optical centre of the imager. the view plane can then be positioned in such a way that a convenient scaling exists between pixel dimensions and real dimensions at the view plane.

Since the location of the view plane is known the 2D image coordinates can be transformed into world coordinates of the projected point at the view plane, the third world coordinate would be some function of x,y , and z of the vtp relative to the prp .

The above methodology is used to find the real world coordinates of the control points at the view plane, since the world coordinates of the prp are also known, vectors can be produced for all control points in the image.

4 Determination of Cloud Spatial Properties

Vectors produced from the 2D ground image are projected onto the satellite image. The satellite image is assumed to be orthographic due to the relative distances involved between the satellite, clouds and Earth. Not all vectors are projected since some represent the height of the cloud rather than the cloud base which is used for matching. The choice of vectors projected depends on the

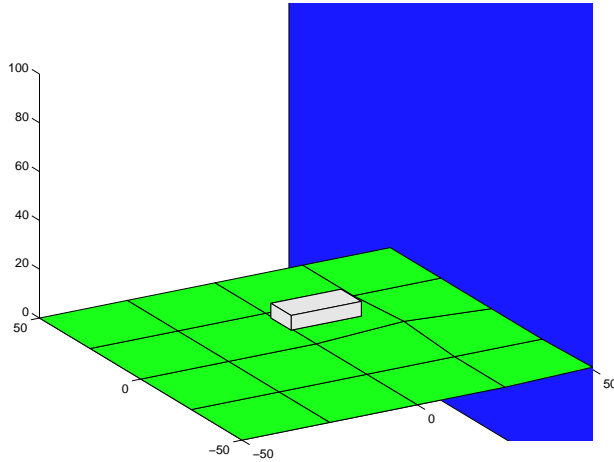


Figure 4: A three dimensional visualisation of a generative single cloud scene.

cloud itself which must be determined from the ground-based image, however selecting one third of control points with the lowest y gradient gives a good matching ratio.

The selected points are projected on to the satellite view at intervals of y . The matching process is based on finding the sum of the squared minimum of distances between the control points and an Active Contour created on the satellite view. The probability of a match at y is described below.

$$d_j = \sum_i \min_k (\underline{x}_{i,j} - f(\bar{x}_{k,t}))^2 \quad (10)$$

$$l(d_j) = \frac{1}{\sqrt{2\pi}\sigma} e^{-\frac{d_j}{2\sigma^2}} \quad (11)$$

$$P(y) = \frac{l(d_j)}{\sum_j l(d_j)} \quad (12)$$

The remaining properties of cloud extent, with the exception of cloud top height, can be found from the satellite image. Cloud thickness is particularly difficult to establish under our methodology using a single ground-based image, this is due to a lack of correlation points and it's determination is not attempted. In future work we plan to use several methods to define cloud top height, including imaging based analysis.

5 Results

Detailed results are presented below for a generative cloud scene with a single cloud to show the stages of our methodology (Figure 4 to Figure 8). Further examples are given of multi-cloud scenes. In the first example of a single cloud scene, the cloud's location is precisely defined as having centre $(0, 14, 0)$ with extent $(10, 6, 20)$ in the x, y, z axes. Results from the algorithm can be seen in Table 1.

6 Conclusion

In this paper we presented a method for the retrieval of cloud spatial properties over large discrete cloud fields. While only generative data was used, we have shown that accurate retrieval of CBH and other cloud spatial properties is a viable solution to the problem of CBH retrieval across cloud

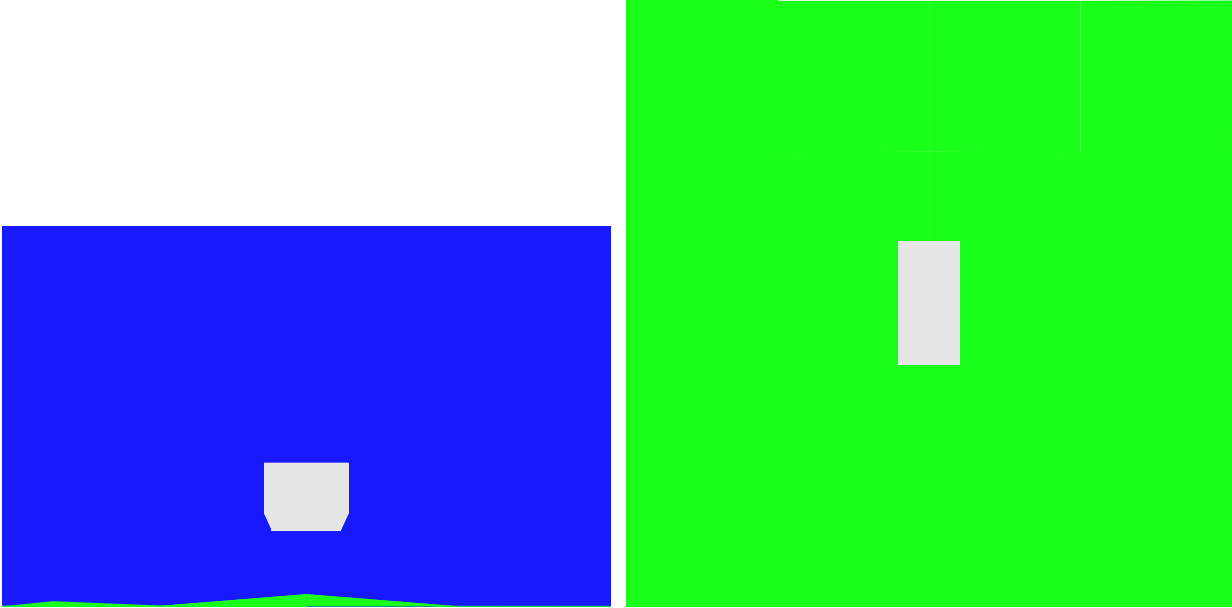


Figure 5: Perspective projections from ground and satellite view points. Edge detection using the Canny edge detector is performed on the green channel of these images before active contours are applied.



Figure 6: The progression of spline control points across both the ground and satellite based views. The active contours' initial position is the smallest ellipse, each successive iteration produces a spline of increasing size, drawn towards the features' edges, until the forces are balanced and the spline converges on it's final shape.

| Cloud Attribute | Retrieved Data | Known Value |
|-------------------|----------------|-------------|
| Cloud Base Height | 11.1000 | 11.0000 |
| x Centre | 0.1843 | 0.0000 |
| z Centre | 0.1639 | 0.0000 |

Table 1: Retrieved cloud spatial properties from a single cloud scene.

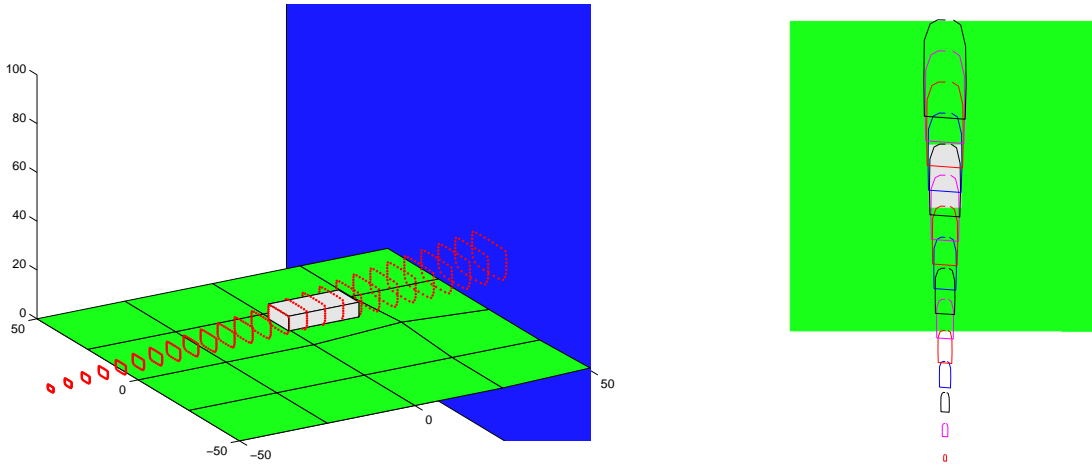


Figure 7: Images showing the projection of control points from the ground-based active contours through space. Shown left is a 3D projection of all control points at intervals of z , right is a projection of the lowest $\frac{1}{3}$ of control points found in the ground-based image onto the satellite image projected at intervals of y .

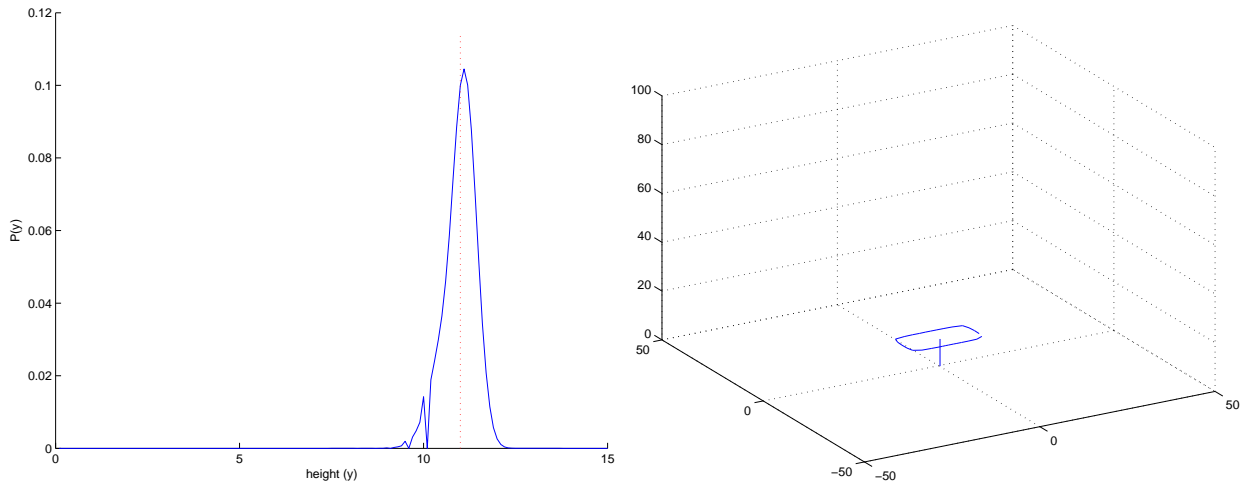


Figure 8: 3D image of retrieved cloud location and plot of probability of matching between the spline shown in Figure 6(right) and splines projected at intervals of y in Figure 7(right), the red dotted line shows the actual height of the cloud. The spline shown(left) is that with the highest $P(y)$.

| Cloud Attribute | Retrieved Data | Known Value |
|-------------------|----------------|-------------|
| Cloud Base Height | 8.8000 | 8.5000 |
| x Centre | -20.0843 | -20.0000 |
| z Centre | -15.0040 | 15.0000 |

Table 2: Retrieved cloud spatial properties from a single off centre cloud scene.

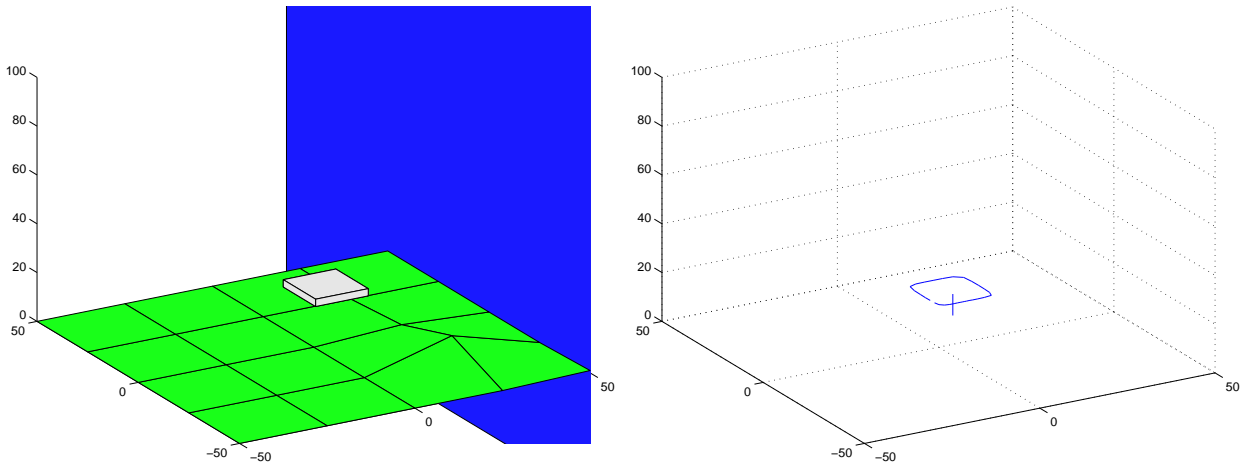


Figure 9: Second example showing generative and retrieved data for an off-center cloud.

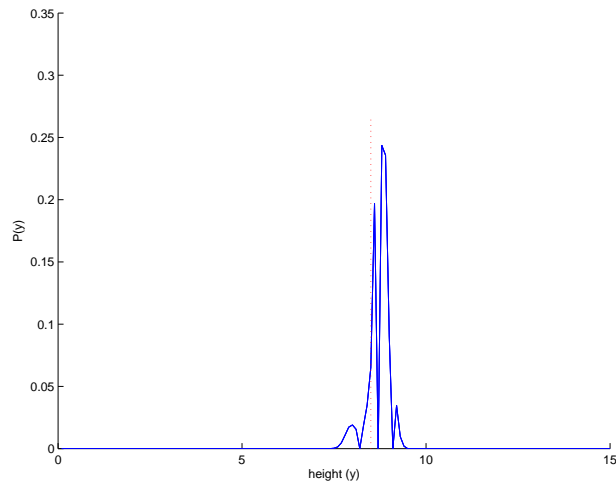


Figure 10: PDF plot showing probability of a match, again the red dotted line shows the actual height.

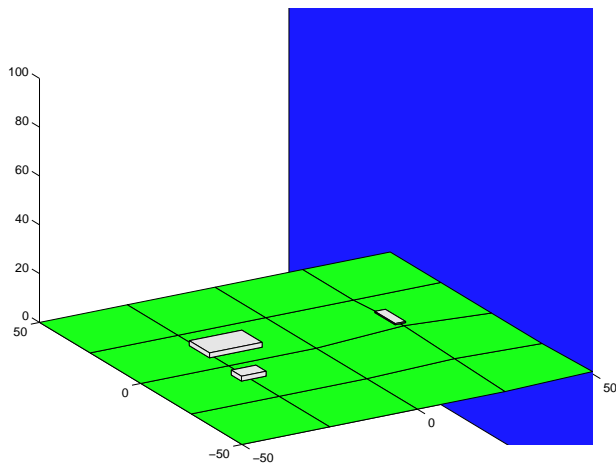


Figure 11: 3D image of a multi-cloud scene.



Figure 12: Images showing the converged active contours overlaid onto pre-processed ground and satellite view images.

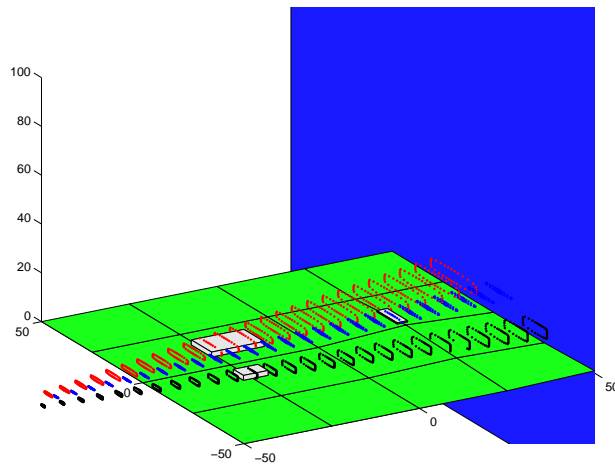


Figure 13: Projections of the active contours found from the ground-based image at intervals of z .

| | Cloud a | | Cloud b | | Cloud c | |
|-------------------|-----------|----------|-----------|---------|-----------|----------|
| Cloud Attribute | Retrieved | Known | Retrieved | Known | Retrieved | Known |
| Cloud Base Height | 1.6000 | 1.5000 | 1.0000 | 1.0000 | 8.0000 | 7.7500 |
| x Centre | -9.8298 | -10.0000 | 10.1642 | 10.0000 | 2.2059 | 2.0000 |
| z Centre | 20.2288 | 20.0000 | 25.2519 | 25.0000 | -19.9952 | -20.0000 |

Table 3: Retrieved cloud spatial properties from the multi-cloud scene shown in Figure 11.

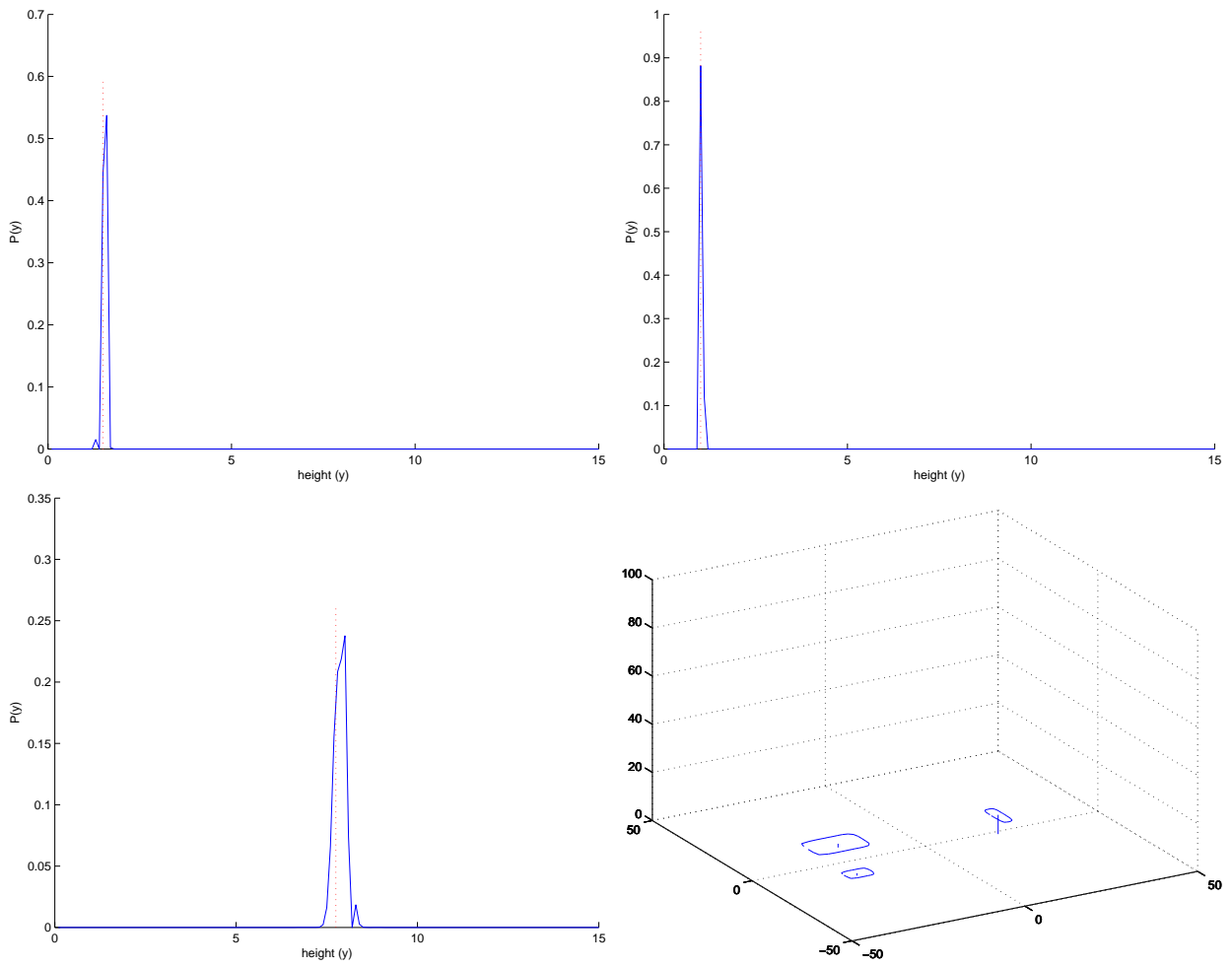


Figure 14: Plots for each of the three clouds in Figure 11, showing their actual CBH (shown by a red dashed line) and the computed CBH probability distribution. Finally the 3D model of the multi-cloud environment.

fields, using ground-based and sat images.

Our results show a highly accurate correlation between the generative data and retrieved values, which as expected, becomes less accurate for clouds at greater distances from the ground-based imager.

In future work we intend to:

- i. Migrate to real-world data, using cheap ‘off-the-shelf’ digital cameras for ground-based imaging and Meteosat-7, visible spectrum data. Use of Meteosat Second Generation data will be considered once the platform becomes operational at the beginning of 2004.
- ii. Automate the system, replacing the need for manual seeding of active contours.
- iii. Incorporate multi-location ground-based imagers with overlapping fields of view to increase the accuracy of the system.
- iv. Expand the system for temporal analysis of cloud fields.

Acknowledgements

This work was funded by the School of Engineering and Applied Sciences, Aston University.

References

- Blake, A. and M. Isard 2000. *Active Contours: The Application of Techniques from Graphics, Vision, Control Theory and Statistics to Visual Tracking of Shapes in Motion* (2nd ed.). Springer.
- Cohen, L. D. 1991. On active contour models and balloons. *Computer Vision, Graphics, and Image Processing. Image Understanding* **53** (2), 211–218.
- Foley, J. D., A. van Dam, S. K. Feiner, and J. F. Hughes 1997. *Computer Graphics: Principles and Practice*. Addison-Wesley.
- Mackiewicz, B. 1995, August. Intracranial boundary detection and radio frequency correction in magnetic resonance images. Master’s thesis, Simon Fraser University. Chapter 5.2.
- Xu, C. and J. Prince 1997, June. Gradient vector flow: A new external force for snakes. In *Proceedings of Computer Vision and Pattern Recognition (CVPR ‘97)*, pp. 66–71. San Juan, Puerto Rico, IEEE.